Supporting Information

Bereiter et al. 10.1073/pnas.1204069109

SI Text

SI Materials and Methods. ***Synchronization of CO_2 records.*** For temporal comparability, we synchronized the data of the Byrd and TALDICE cores to the EDML1 Scenario 4 gas age scale (1) by matching the tie points (Fig. 1) in the CH_4 records of the different ice cores, based on the work of ref. 2. Between the tie points, the age scales for Byrd and TALDICE have been linearly interpolated. We used the same principle for the Taylor Dome data (3) but in an indirect way. Here, we translated the age scale of ref. 4, for which a synchronization with Taylor Dome data exists. This indirect synchronization is less suitable for our purposes for two reasons: First, we do not know the uncertainties of the synchronization between the Byrd and Taylor Dome data; second, CO_2 matching has been partly applied in that synchronization, which is less precise due to the rather slow atmospheric CO_2 changes. To better identify the tie points in the TALDICE record around DO 17 to 14, we used new highly resolved CH_4 data measured with a continuous flow analysis technique (5). Tie points are identified where rapid CH_4 changes occur and their location is thus not dependent on the absolute values of CH_4, which may differ in ref. 5 from those in ref. 2. If possible, we matched the midpoints of the CH_4 change, otherwise maxima associated with DO-events are used.

Offsets between CO_2 records. Several issues have to be taken into account when comparing CO_2 records from different ice cores and measured in different labs:

i. Different analytical methods and independent standardization can lead to interlaboratory offsets. Moreover, non-linearities in the standardization may lead to offsets that can depend on the mean CO_2 concentration, if those non-linearities are not corrected.
ii. The ice core gas records are given on age scales that are CH_4 synchronized using best practice approaches; however, smaller synchronization errors on the order of a few centuries may still exist, especially for time periods where no synchronization tie points exist. This may lead to offsets in concentrations away from intervals of stable CO_2 levels and away from tie points.
iii. The different enclosure characteristics of various ice cores lead to a different damping of fast CO_2 changes. Thus, a direct comparison of CO_2 levels from different ice cores is only unambiguous for CO_2 changes that last significantly longer than the width of the age distribution of the air bubbles in the ice. In the cores used here, this width is on the order of a few centuries, with Taylor Dome having the widest and Byrd the narrowest glacial age distribution. Accordingly, the amplitude of changes in maxima and minima can be different in ice cores if concentration variations are short-lived. Another effect related to the firnification process is gravitational enrichment of CO_2 relative to N_2. This effect leads to an enrichment on the order of 1–2 ppmv at the bubble close-off depth. The size of this effect depends on the depth of the diffusive firn column at the different sites. Accordingly, we estimate this effect to explain offsets between individual cores of maximum 1 ppmv. Also atmospheric CO_2 concentration changes could lead to a diffusive enrichment/depletion, if the firn column is not in CO_2 equilibrium with the atmosphere. The CO_2 changes observed in our records, however, are too slow for this to be the case.
iv. A clear fractionation between CO_2 and the main air components has been observed in the bubble clathrate transition zone (BCTZ) (6). Here, CO_2 is preferentially included into clathrates, leading to an enrichment in the integrated clathrate CO_2 content and a depletion in the remaining integrated bubble content. Due to the incomplete extraction efficiency of dry extraction techniques, the air enclosed in remaining bubbles is preferentially released. Thus, techniques with different extraction efficiencies lead to offsets in the CO_2 concentration for BCTZ ice and high scatter in the data (6). Here, we used only ice well below the BCTZ to minimize the bubble/clathrate fractionation problem. Moreover, large clathrates are formed later in the clathrate formation process (i.e., deep in the BCTZ) than smaller ones (7). Also the CO_2 content in clathrates is expected to be highest in (small) clathrates formed at the top of the BCTZ and decrease with depth as is the case for the O_2/N_2 ratio (7). Thus, the CO_2 content of large and small clathrates might be different within the BCTZ. Below the BCTZ, diffusion in the ice slowly re-equilibrates the clathrates (6). This process, however, requires several millennia. Accordingly, preferential extraction of gas entrapped in large clathrates just below the BCTZ using dry extraction techniques can lead to a similar albeit smaller depletion in CO_2 concentration, as is the case in mixed bubble/clathrate ice from the BCTZ.
v. The storage time for different ice cores differs. For example, the Byrd ice core has been stored in cold rooms at only −20 °C for nearly 40 y before the analyses performed (4). In this time, many clathrates relax back to bubbles, during which a fractionation of gases may occur again. In summary, offsets between different ice core measurements may also be due to a different stage of the clathrate relaxation process. Based on our observations of CO_2 enrichment in clathrates in the BCTZ, we would expect the reverse fractionation to occur during this relaxation. Accordingly, the integrated CO_2 content should be depleted in the reformed bubbles. The more complete the relaxation process is, the less depleted the integrated bubble content should become in CO_2. However, also net gas loss has been observed in ice stored at higher temperatures (8). This would lead to a net enrichment of the CO_2 concentration in the ice, which becomes stronger the more O_2 is lost from the ice. Careful sample selection away from the outer surface of the ice core (where loss processes play the strongest role), as done in our analyses, helps to minimize this effect (9).
vi. Finally, also in situ CO_2 production by oxidation of organic acids and carbonate-acid reaction, as notoriously observed in Greenland ice (10, 11), can also not be ruled out entirely for Antarctica. This effect is estimated to be smaller than 1.5 ppmv for Antarctic ice (9).

Given this long list of processes that can influence the CO_2 concentration in Antarctic ice cores, it is not surprising to observe differences between different labs and ice cores of a few ppmv. Fig. 1 in the main text shows that the different records agree in the temporal changes in CO_2, but not in the mean level of CO_2 concentrations. Moreover, these offsets are not always constant over the entire records.

In the following, we concentrate on a few features in these offsets and provide potential explanations. Note however, that the relative temporal changes in CO_2 discussed in the main text are seen in all records and, thus, the small offsets do not affect our conclusions drawn on the phasing between DO event onsets and CO_2.

i. The TALDICE CO_2 data are in reasonable agreement with the Byrd record (4) in the amplitude of the large CDM events. Small deviations during the increasing and decreasing flanks of CDM can be explained by the synchronization errors. The existence of small-scale variations in the TALDICE record not seen in Byrd in connection to DO 9–11 can be mainly attributed to the higher resolution of the TALDICE record and partly to storage effects in the old Byrd ice core. A good agreement between those two cores is not necessarily to be expected in view of the significant clathrate relaxation in Byrd ice during the long storage time. If the relaxation process is connected to a fractionation as suggested above, then the good agreement between the TALDICE measurements performed here and the Byrd ice measurements performed by ref. 4 shows that either the extraction technique used by ref. 4 does not fractionate between gas entrapped in bubbles and clathrates or that the relaxation was nearly complete. In the latter case the remaining net fractionation in bubble air is small. Interestingly, measurements were performed on the Byrd core also in Bern in the late 1980s (12); i.e., 20 y earlier than by ref. 4 but still after two decades of storage. These earlier measurements showed significantly lower (about 10 ppmv) and more scattered CO_2 concentrations than in ref. 4 and are also lower than measurements on pure bubble ice from the Taylor Dome ice core (3). These lower CO_2 values could be explained by a significant fractionation during the still more incomplete relaxation process in Byrd ice 20 y ago. Moreover, the extraction method at that time was not yet optimized for clathrated ice and the extraction efficiency of air from clathrates was even lower than with our current method. Accordingly, a stronger CO_2 depletion of air preferentially released from bubbles or large clathrates with the old technique is to be expected.
ii. The Taylor Dome measurements performed on pure bubble ice appear to be in line with the TALDICE ice core for some periods (40–55 kyr BP) and to be about 5 ppmv too low in others (55–65 kyr BP). However, this record is of comparatively low resolution and the synchronization is not perfect, explaining most of the differences. Moreover, the glacial Taylor Dome ice has a more than two times wider gas age distribution and smaller amplitudes of CO_2 change are to be expected in this core.
iii. Finally, we observe on average about 4 ppmv lower CO_2 concentrations in the EDML ice core compared to TALDICE over the time interval 45–65 kyr BP. For earlier time periods, the EDML record is in reasonable agreement with Byrd (4), except for the peak at DO 19, which is significantly lower in the EDML record. The latter could partly be explained by the wider gas age distribution in EDML compared to Byrd; however, a similar difference is not observed for the variations in CO_2 concentration prior to DO 19. Future analyses on other cores will have to show, which of the CO_2 concentration values over CDM 19 is correct.
iv. The small but significant difference between the TALDICE and the EDML records appears to be harder to explain. It may be related to the clathrate formation in the BCTZ. As outlined above large clathrates formed deep in the BCTZ might store less CO_2 than smaller ones. Since our extraction system (dry extraction with needle cracker) preferentially opens bigger enclosures (bubbles or clathrates), we would measure slightly lower concentrations in samples just below the BCTZ compared to values from other ice cores of the same age far below the BCTZ. The fractionation will vanish with time and distance to the BCTZ due to diffusive gas exchange (6) between the clathrates. Since this equilibration is faster in the TALDICE record as in the EDML record (6), it could explain the tendency of the EDML data to be slightly lower than TALDICE during CDM 14 to 17 (Fig. 2). Alternatively, the longer storage time (and, thus, stronger clathrate relaxation) of EDML ice (3–6 y) compared to TALDICE ice (0.5–3 y) could explain the slightly lower CO_2 concentrations. Long-term replicate CO_2 monitoring on stored ice from the same ice core should be able to document such a long-term storage and relaxation effect.

Identifying the trigger for the DO onset. The rapid temperature increase at the DO onset causes a sharp increase of CH_4 concentrations in the atmosphere within 50 y (13). Therefore, high-resolution CH_4 records can be used to precisely determine DO onsets in the gas enclosed in ice cores. Gas enclosure characteristics have the potential to shift and dampen atmospheric variations in the gas composition (14). A broad age distribution of the enclosed gas favors rapid changes in gas compositions to be dampened and shifted forward relative in time. If that effect would have significantly influenced our records, the CH_4 jumps used to identify the DO-events would have been shifted forward in time more strongly than the CDM due to the faster change rates of CH_4 at that time. Accordingly, a possible lag of CDM relative to the CH_4 jump would be underestimated. Furthermore, accumulation rates are smaller during MIS 3 than during MIS 5 (15, 16), which results in a broader age distribution of the enclosed gases during MIS 3 than during MIS 5. Hence, this change would favor a stronger shift forward in time of the CH_4 jump relative to the CDM during MIS 3 compared to MIS 5. Thus, our findings on the CDM phase lag difference between MIS 3 and 5 can be regarded as conservative. However, neither are the accumulation rates during both periods and in both cores low enough nor are the changes from MIS 5 to MIS 3 large enough that a significant shift of the CH_4 jumps is to be expected.

The onset of the DO events (point zero in Fig. 2)–for which we found a corresponding CDM–has been identified as the midpoint between the first significantly increased CH_4 value and the data point before that (Fig. S1). This has been done using the highest resolved CH_4 data available for the corresponding period and independently for the TALDICE and EDML ice core records. The uncertainty of this time marker was defined as half of the temporal difference between the two CH_4 data points around the marker.

Splines of CDM and CO_2 change rates. To calculate robust values for the delay of CDM with respect to the corresponding DO onset, we computed 500 Monte Carlo splines (see main text) with 500 y and 1,000 y cut-off period for each CDM in our records with data points randomly varied within the measurement uncertainty. From these, we calculated an average spline and its confidence interval for each CDM and each cut-off period (Fig. S2 and 3). The cut-off period defines the frequency, which is damped to 50% in the frequency spectrum of the splines with stronger dampening for higher frequencies (17). To calculate delays of CDM with respect to the DO onset, we used the results with 500 y cut-off period since the 1,000 y cut-off period splines dampen the peaks of the CDM, which results in larger uncertainties of the calculated delays. Rates of change of atmospheric CO_2 are calculated based on spline results with a 1,000 y cut-off period (Fig. S3) as variations caused by single data points are reduced here.

To calculate rates of changes before CDM, the largest possible window of steady rates of changes before each splined CDM has been selected and linearly interpolated (black lines in Fig. S3). For MIS 3, rates of change of CDM 12, 14, and 17 of the TALDICE record have been used since the TALDICE record shows higher data quality during this time period (*Methods*). For MIS 5 only CDM 20, 21, and 24 have been used, as CDM 23 and 19 have much smaller amplitudes as the other events and rates of change are exceptionally small at CDM 23 and given over a very small time window at CDM 19 (only two data points included)

(Table S1). Based on these six values, an average rate of change before a CDM of 6.1 ± 0.6 ppmv/kyr for MIS 3, and 14.6 ± 3.7 ppmv/kyr for MIS 5 is found. On the one hand, the values of CDM 19 and 23 are excluded and, hence, the validity of the MIS 5 value can be challenged. On the other hand, if all events during MIS 5 are included the average rate of change is at 12.2 ± 2.8 ppmv/kyr and the four highest rates of change are found during MIS 5 (Table S1). Based on these results, it appears that rates of change before CDM are larger for MIS 5 than for MIS 3.

Significance test of the difference in the CDM delay between MIS 3 and MIS 5. To determine the statistical significance of the different delays of CDM relative to the DO onsets between MIS 3 and MIS 5, the null hypothesis that the delay of CDM relative to the DO onset is equal for MIS 3 and MIS 5 was tested against the hypothesis that this delay is greater during MIS 3 than MIS 5 using a conservative strategy. For each CDM, the delay relative to the DO onset and its uncertainty was determined based on the Monte Carlo splines with 500 y cut-off period (Table S2). To the uncertainty of the delay derived from the splines, the maximum uncertainty in the onset of the DO-event trigger was added (defined by the time interval between the two CH_4 data points defining the onset, Fig. S1). Note that this is a conservative estimate, since the uncertainty of the delay and of the DO onset trigger are independent of each other. This defines a new delay uncertainty for each event in MIS 3 and MIS 5 shown in Fig. 2 (top boxes) and Table S2. Using these new uncertainties, a Monte Carlo simulation was performed producing 1,500 possible values for each event. The mean and the standard deviation over all values for the MIS 3 and MIS 5 period, respectively, were calculated and tested in an independent two-sample *t*-test.

A first conservative approach is to use only results based on the EDML record since it is the only record that covers all events and, hence, all delays originate from the same ice core. This approach results in a *t*-value of 1.85 which is slightly lower than the critical *t*-value for a one-sided test with 6 degrees of freedom and 95% significance (1.94) and higher than the one for 90% significance (1.44). However, a Wilcoxon rank sum test (or Mann-Whitney U test) using the means of each CDM shows a significance above 95%.

The EDML record has two weaknesses which influence the delay for MIS 5 CDM using this splining strategy: First, the resolution of CDM 24 is rather coarse for the 500 y cut-off period spline. Second, CDM 23 has both an exceptional large uncertainty (see Fig. 2) due to the smaller amplitude and a DO trigger that can be questioned (Fig. S1). When CDM 24 from the EDC record (18) is added–no matter if we include CDM 23 or not–the rank sum tests show a clear significance above 95%. This is also true for the *t*-test when CDM 24 is included but CDM 23 excluded. If both CDM are included, the significance is just around 95%.

So far, no data from the TALDICE ice core has been taken into consideration for these significance tests. Due to the higher quality of the TALDICE records, the delay estimates of the MIS 3 type events are more precise as the ones derived from the EDML records. In a last step, the estimates from the TALDICE records are used as additional independent measures of the delay of MIS 3 type events. Using the TALDICE delays, the significance is above 97.5 % (*t*-value = 2.50; critical *t*-value for 97.5% significance and 10 degrees of freedom = 2.23).

In summary, this means that CDM of MIS 3 show a larger delay relative to their corresponding DO event onsets than CDM of MIS 5 with a significance around 95%, using EDML data only. However, the estimates derived from the EDC and TALDICE records can be used as independent measure of the delay of MIS 3 and MIS 5 type events increasing the significance above 97.5%.

1. Loulergue L, et al. (2007) New constraints on the gas age-ice age difference along the EPICA ice cores, 0–50 kyr. *Clim Past* 3:527–540.
2. Schilt A, et al. (2010) Atmospheric nitrous oxide during the last 140,000 years. *Earth Planet Sci Lett* 300:33–43.
3. Indermühle A, Monnin E, Stauffer B, Stocker TF, Wahlen M (2000) Atmospheric CO_2 concentration from 60 to 20 kyr BP from the Taylor Dome ice core, Antarctica. *Geophys Res Lett* 27:735–738.
4. Ahn J, Brook EJ (2008) Atmospheric CO_2 and climate on millennial time scales during the last glacial period. *Science* 322:83–85.
5. Schüpbach S, Federer U, Bigler M, Fischer H, Stocker TF (2011) A refined TALDICE-1a age scale from 55 to 112 ka before present for the Talos Dome ice core based on high-resolution methane measurements. *Clim Past* 7:1–16.
6. Lüthi D, et al. (2010) CO_2 and O_2/N_2 variations in and just below the bubble-clathrate transformation zone of Antarctic ice cores. *Earth Planet Sci Lett* 297:226–233.
7. Salamatin AN, Lipenkov VY, Ikeda-Fukazawa T, Hondoh T (2001) Kinetics of air-hydrate nucleation in polar ice sheets. *J Cryst Growth* 223:285–305.
8. Bender ML (2002) Orbital tuning chronology for the Vostok climate record supported by trapped gas composition. *Earth Planet Sci Lett* 204:275–289.
9. Bereiter B, Schwander J, Lüthi D, Stocker TF (2009) Change in CO_2 concentration and O_2/N_2 ratio in ice cores due to molecular diffusion. *Geophys Res Lett* 36:1–5; AGU doiidentifier: L05703 doi: 10.1029/2008GL036737.
10. Anklin M, Barnola J, Schwander J, Stauffer B, Raynaud D (1995) Processes affecting the CO_2 concentrations measured in Greenland ice. *Tellus* 47B:461–470.
11. Smith HJ, Wahlen M, Mastroianni D (1997) The CO_2 concentration of air trapped in GISP2 ice from the last glacial maximum-holocene transition. *Geophys Res Lett* 24:1–4.
12. Neftel A, Oeschger H, Staffelbach T, Stauffer B (1988) CO_2 record in the Byrd ice core 50,000–5,000 years BP. *Nature* 331:609–611.
13. Huber C, et al. (2006) Isotope calibrated greenland temperature record over marine isotope stage 3 and its relation to CH_4. *Earth Planet Sci Lett* 243:504–519.
14. Spahni R, et al. (2003) The attenuation of fast atmospheric CH_4 variations recorded in polar ice cores. *Geophys Res Lett* 30:1–4; AGU identifier: 1571 doi: 10.1029/2003GL017093.
15. Ruth U, et al. (2007) "EDML1": A chronology for the EPICA deep ice core from Dronning Maud Land, Antarctica, over the last 150,000 years. *Clim Past* 3:475–484.
16. Buiron D, et al. (2011) TALDICE-1 age scale of the Talos Dome deep ice core, East Antarctica. *Clim Past* 7:1–16.
17. Enting IG (1987) On the use of smoothing splines to filter CO_2 data. *J Geophys Res* 92:10977–10984.
18. Schneider R (2011) Quantifying past changes of the global carbon cycle based on $\delta^{13}CO_2$ measurements in Antarctic ice cores. PhD thesis (Univ of Bern).

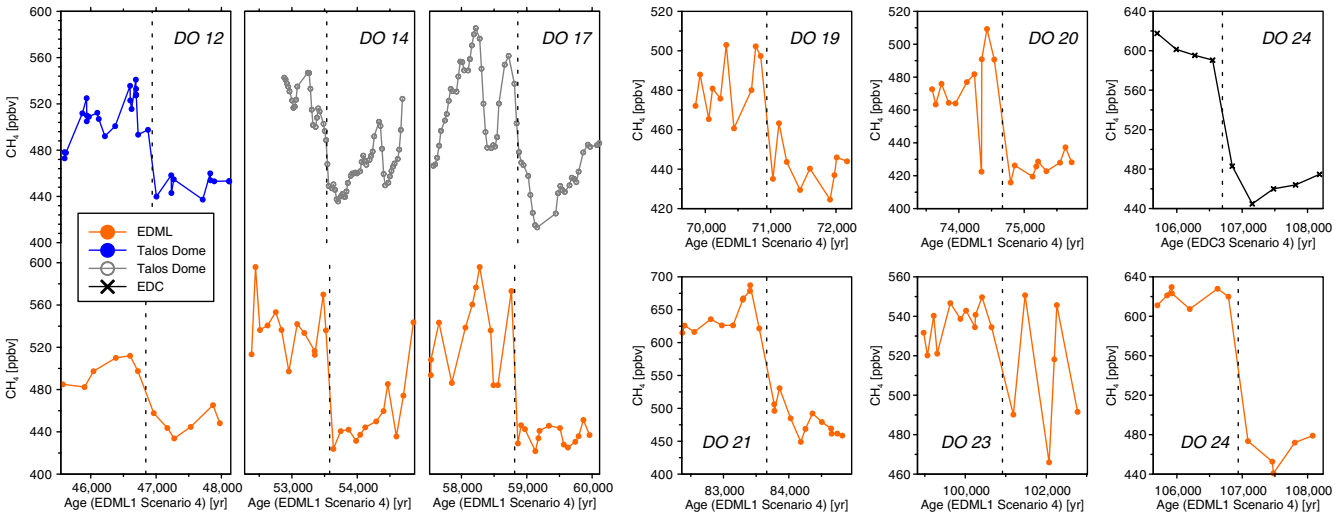

Fig. S1. Compilation of CH_4 records used to identify the onset of DO events. Left three boxes: CH_4 records of DO-event number 12, 14, and 17 from TALDICE [blue (1) and gray (2)] and EDML [orange (3–5)] ice core. Right six boxes: CH_4 records of DO event number 19, 20, 21, 23, and 24 from EDML [orange (3, 5)] and EPICA Dome C [EDC; black (6)]. TALDICE and EDML data are plotted on the EDML1 Scenario 4 age scale; EDC on the EDC3 Scenario 4 age scale (7).

1 Buiron D, et al. (2011) TALDICE-1 age scale of the Talos Dome deep ice core, East Antarctica. *Clim Past* 7:1–16.
2 Schüpbach S, Federer U, Bigler M, Fischer H, Stocker TF (2011) A refined TALDICE-1a age scale from 55 to 112 ka before present for the Talos Dome ice core based on high-resolution methane measurements. *Clim Past* 7:1–16.
3 Schilt A, et al. (2010) Atmospheric nitrous oxide during the last 140,000 y. *Earth Planet Sci Lett* 300:33–43.
4 Capron E, et al. (2010) Synchronizing EDML and NorthGRIP ice core using d^{18}O of atmospheric oxygen (d$^{18}O_{atm}$) and CH_4 measurements over MIS5 (80–123 kyr). *Quat Sci Rev* 29:222–234.
5 EPICA Community Members (2006) One-to-one coupling of glacial climate variability in Greenland and Antarctica. *Nature* 444:195–198.
6 Loulergue L, et al. (2008) Orbital and millennial-scale features of atmospheric CH_4 over the past 800,000 y. *Nature* 453:383–386.
7 Loulergue L, et al. (2007) New constraints on the gas age-ice age difference along the EPICA ice cores, 0–50 kyr. *Clim Past* 3:527–540.

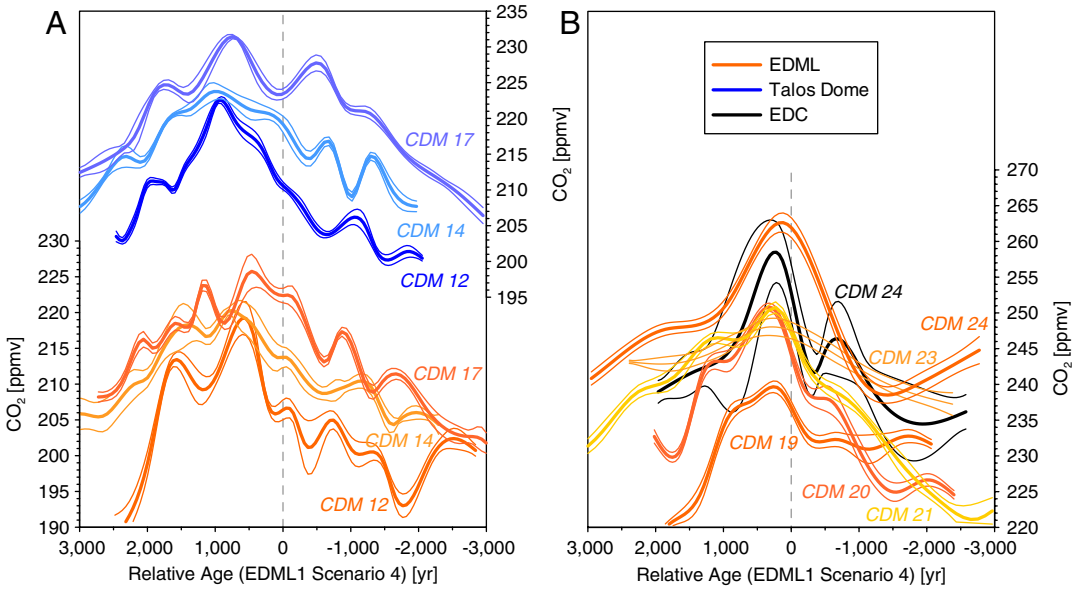

Fig. S2. Splines through CDM with 500 years cut-off period. Thick lines show average splines whereas the thin lines represent the one sigma confidence interval. Blue lines show results from TALDICE data, orange from EDML data and black from EDC. In the left box, the bottom *y*-axis is valid for EDML splines and the top *y*-axis for TALDICE splines.

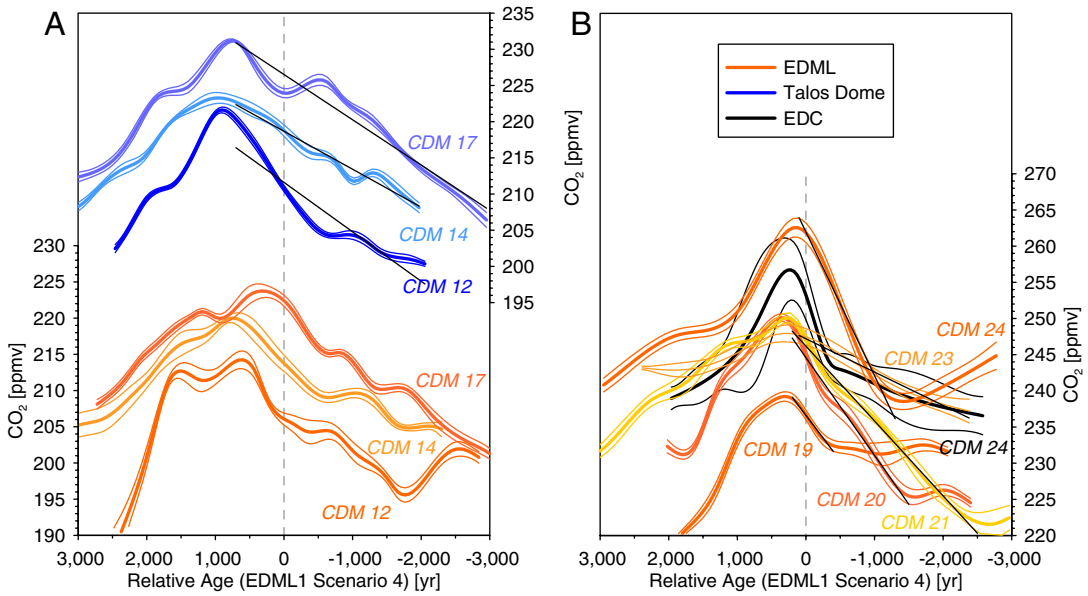

Fig. S3. Splines through CDM with 1,000 y cut-off period. Line, color, and axis affiliations are equal to Fig. S2. Black lines show linear regressions of the corresponding average splines. For the calculation of the regression, the period for which the black lines are plotted has been used. Slopes of the regressions are given in Table S1.

Table S1. Results or linearly interpolated rates of change prior to the peak of the CDM. Values for CDM 12, 14, and 17 are based on TALDICE records; values for CDM 19, 20, 21, 23, and 24 are based in EDML records. The window of linear interpolation is indicated by the black line in Fig. S3

CDM Nr.	12	14	17	19	20	21	23	24
Rates of change [ppmv/kyr]	6.8	5.2	6.3	(12.5)	13.5	10.3	(4.6)	19.9

Table S2. Calculated mean delays of CDM with respect to their corresponding DO event and associated errors (units = years) (Fig. 2)

	CDM Nr.	12	14	17	19	20	21	23	24
EDML	Mean	599	856	540	270	328	251	325	145
	error (σ)	252	387	334	157	160	140	486	172
TALDICE	Mean	927	943	737	-	-	-	-	-
	error (σ)	91	155	87	-	-	-	-	-
EDC	Mean	-	-	-	-	-	-	-	269
	error (σ)	-	-	-	-	-	-	-	327